Consolidation of Sheared, Strongly Flocculated Suspensions

Claes Holmqvist
STFI-Packforsk, 11486 Stockholm, Sweden

Anders Dahlkild
KTH Mechanics, Royal Institute of Technology (KTH), 10044 Stockholm, Sweden

DOI 10.1002/aic.11419
Published online February 8, 2008 in Wiley InterScience (www.interscience.wiley.com).

The concept of a particle concentration dependent yield stress, previously employed in studies of uniaxial consolidation of a flocculated solid phase dispersed in a liquid, is extended to comprise flocculated phase shear strength. The inter-particle stresses are modeled by assuming that the stress state is always located on a yield-surface in stress-space, whose form is adopted from the Cam-clay plasticity theory for the quasi-static consolidation of soil. By treating the time-dependent dewatering of a suspension trapped between a permeable filter and a sliding piston, as well as the asymptotic limit of a cross-flow filtration situation, the differences with respect to the conventional uniaxial models are made apparent, and the effects of the shear stresses on the consolidation process are elucidated. Applying shear is predicted to increase the rate of the drainage process, because of a reduced load bearing capacity of the flocculated phase, and the correspondingly higher pore pressures. © 2008 American Institute of Chemical Engineers *AIChE J,* 54: 924–939, 2008

Keywords: filtration, yield stress, shear, piston, cross flow, critical state

Introduction

The separation of the liquid and solid contents of a suspension has widespread practical importance, and the task can be undertaken by, e.g., subjecting the suspension to a gravity field (sedimentation) or by pressure filtration. In many situations, not only the rate of the process is important, but also the morphology of the separated particle phase. Among the many examples of application areas, one finds fields as diverse as ceramics production, mineral processing, sludge treatment and paper manufacturing.

Historically, gravitational thickening has received more attention than pressure filtration. Kynch[1] presents a kinematic theory of batch sedimentation based on the continuity equation of the solid phase. His main assumption is that the local flux of particles is a function of the local volume concentration of solids ϕ only. Long-range hydrodynamic forces are hence not accounted for by the Kynch theory, and neither is the possibility that stresses are transmitted through the particle phase. The latter interactions have traditionally been accounted for by introducing a "particle pressure", dependent upon ϕ, in the mathematical description of the separation process. In this way, a dependence of the flux on the gradient of ϕ is obtained. In a flocculated suspension, which is the kind that is of primary concern to this study, the origin of the particle pressure is the mechanical contact between the particles. Other possibilities exist, however. As an example, in the case of a stable colloidal suspension the particle pressure corresponds to the osmotic pressure. The first study of settling of a flocculated suspension incorporating particle stresses seems to have been the one by Michaels and Bolger.[2] The authors performed an analysis in which a constant uniaxial yield stress was employed. Early works that include concentration dependent particle stresses are the ones by Shirato et al.[3] and Adorján.[4]

The Kynch analysis predicts the formation of discontinuities in ϕ during the settling process. According to Auzerais

Correspondence concerning this article should be addressed to C. Holmqvist at claes.holmqvist@stfi.se.

et al.,[5] the nature of these discontinuities has been much debated. By retaining both inertial effects and inter-particle stresses in the momentum balance of the batch settling problem, in addition to viscous drag and gravity, they are able to show by scaling arguments when approximate discontinuities in ϕ can be expected. In the case these are caused by stresses transmitted by the particles, the controlling parameter is a Péclet number, *Pe*, expressing the magnitude of gravity to inter-particle forces. Sharp gradients, separating regions where Kynch's theory is valid, only occur for large *Pe*. The analysis by Auzerais et al.[5] also resolves the ambiguities previously involved in finding solutions by Kynch's method. Employing the technique of matched asymptotic expansions to the transient settling of a colloidal suspension, Davis and Russel[6] obtain a solution valid in all regions of the suspension for large values of the relevant *Pe*.

In their studies of sedimentation of flocculated suspensions, Buscall and White,[7] Landman et al.[8] and Howells et al.[9] argue that for sufficiently high solids concentrations, the flocs form an interconnected network that can withstand external forces. To describe this they introduce a concentration dependent yield stress, which is defined as the value of the network stress above which the load cannot be balanced by elastic stresses in the solid phase. The network will then consolidate irreversibly. Unlike, e.g., Adorján,[4] they do not assume *a priori* that the particle pressure equals the yield stress. However, it is found that if the rate of consolidation of the solid phase is limited by the drainage of fluid between the particles, rather than the breaking and reformation of particle–particle bonds, this is likely to be a very good approximation. The same concept is used by Landman et al.,[10] Landman and Russel,[11] and Landman et al.[12] to model particle stresses during pressure filtration, as well as in the most recently published works on separation.[13–16] Experimental observations of yield-stress and elastic properties of some strongly flocculated colloidal suspensions are presented by Buscall et al.,[17,18] and Channell and Zukoski.[19] Notably, the suspensions are observed to possess finite yield-limits in both shear and uniaxial compression.

All the hitherto cited theoretical studies of pressure filtration deal with uniaxial filtration, in which only normal loads are applied to the network of flocculated particles. However, in certain applications, the network is subjected also to shear loads. It is a reasonable assumption that these additional load components influence the ability of the solid structure to resist the normal load, since they increase the strain on the inter-particle bonds. Practical experience confirms that combining normal and shear loads does indeed have a favorable effect on separation rates.[20] Further, the displacements of the suspension constituents are not necessarily restricted to a single direction. It is evident that, to cover additional filtration applications, a more general model is needed for the stresses and strain-rates in the flocculated network, than is provided by the above previous works.

Gustavsson[20] presents a model for consolidation, in which it is assumed that the inter-particle forces manifest themselves as both an isotropic strain-rate independent stress, and deviatoric viscous stresses. The model is used in a two-dimensional context to consider settling by gravity of a suspension contained in a closed vessel, while shear is applied to the sediment on the deposition surface. Deviatoric rate-independent stresses are however not taken into account.

For granular flows, Savage[21] puts forward the proposition that, in the intermediate regime where both short-time collisions and continuous contacts occur between particles, the total stresses might be represented as the linear sum of a rate-independent frictional part and a viscous part obtained from the theory for the fully dynamic rapid flow regime. More detailed treatments based on this concept are performed by Johnson and Jackson[22] and Johnson et al.[23] The models for the frictional stress tensor are taken from the discipline of soil mechanics, where plasticity models have been developed for the yielding of porous media under general load conditions (cf. the standard textbooks[24]). Soil plasticity theory, combined with elasticity, is also employed by Zhao et al.[25] for an analysis of wall effects in a Compression-Permeability Cell*, and by Owen et al.[26] to study the rolling of prepared sugar cane. However, these works do not address the effects of applying shear loads, nor the role played by the deviatoric stresses in the model.

In the present study we add the divergence of a strain-rate independent stress tensor representing inter-particle forces to the momentum balance for a mixture of solid particles and liquid. For these stresses, a plastic constitutive theory is adopted from the field of soil mechanics. In this way, it is possible to generalize the yield-stress concept previously employed for uniaxial consolidation to also include the shear strength of the flocculated particle structure. As a result of the choice of constitutive theory, external loads transmitted to the solid phase can only be balanced by strain hardening because of volumetric compression. At certain ("critical") stress states, resulting in isochoric deformations, this mechanism is not at work and the deviatoric deformation rates become undefined. To overcome this limitation, viscous deviatoric stresses are also attributed to the particle phase in the model. By applying the model to two types of plane sheared consolidation, its differences with respect to the conventional models are made apparent, and the effects of the shear stresses on the consolidation process are elucidated.

Formulation

Two different filtration problems are considered. First, a piston driven consolidation is studied, where the flocculating suspension is trapped between a solid, sliding piston, and a permeable filter (cf. Figure 1a). In the second problem, the sliding piston is replaced by a cross-flow of a body of liquid pressed through the flocculated suspension trapped by the filter below (cf. Figure 1b). The mathematical treatment of these problems is detailed below, utilizing their principal similarities.

We first turn to the piston-driven consolidation. The plates constituting the piston and the filter are assumed to lie in a horizontal *xz*-plane, and to be rigid, parallel and of infinite extension. The piston is impermeable to both the liquid and the particle phase of the suspension, whereas the filter is impermeable only to the particle phase, and perfectly permeable to the liquid phase. The initial volume fraction of solids, ϕ_0, is assumed homogeneous and higher than the gel point $\phi = \phi_g$ at which the solid phase first starts to form an interconnected network. Consequently, the entire space between the plates is filled with a flocculated network having an inner

* These devices are used for uniaxial consolidation experiments.

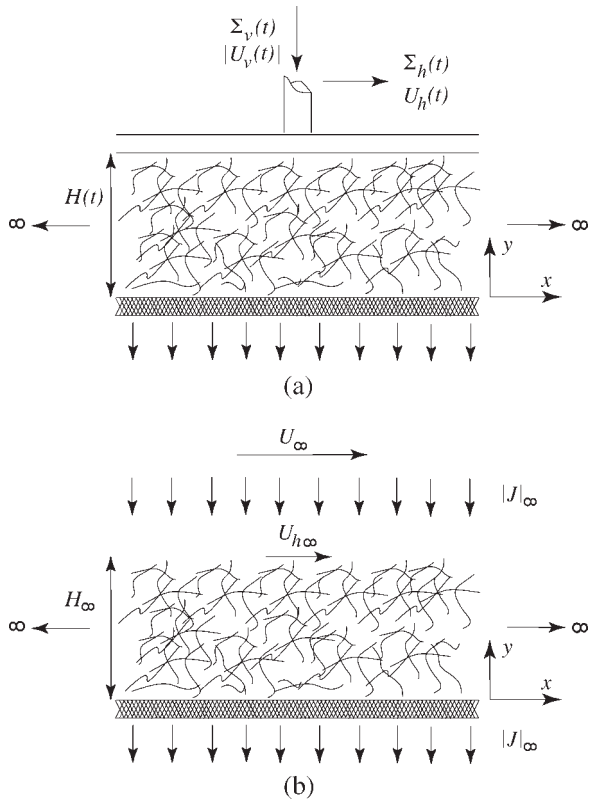

Figure 1. (a) Piston driven filtration; (b) cross-flow filtration; asymptotic limit.

The two considered filtration applications. The piston driven consolidation is controlled by specifying either the load ($\Sigma_v(t)$, $\Sigma_h(t)$) by which the piston is applied to the suspension, or its velocity ($U_h(t)$, $U_v(t)$). A combination of the two modes of control is also possible. During the cross-flow filtration, the vertical, and horizontal loads on the fiber mat are generated by exposing the mat to a free stream flow with vertical and horizontal asymptotic components J_∞ and U_∞, respectively.

strength and capable of bearing certain loads. While the filter is fixed at $y = 0$, the piston is movable and its position $y = H(t)$ is a function of time. Its movements, which in the present study will be limited to the xy-plane, are either controlled by specifying the vertical (i.e., in the y-direction) and horizontal (in the x-direction) loads by which it is applied to the suspension, $\Sigma_v(t)$ and $\Sigma_h(t)$, respectively, or by specifying its corresponding velocity components $U_v(t)$ and $U_h(t)$, respectively. A combination of the two modes of control can also be envisaged, one could, e.g., specify $\Sigma_v(t)$ and $U_h(t)$.

As the resistance to liquid flow through the filter is zero, the liquid pressure p_c must there equal the ambient pressure, which is arbitrarily set to zero,

$$p_c(y = 0) = 0. \tag{1}$$

Both components of the particle phase velocity, denoted $\boldsymbol{u}_d$, are zero at the filter, as is the horizontal component of the liquid phase velocity, $\boldsymbol{u}_c$,

$$\boldsymbol{u}_d(y = 0) = \boldsymbol{0}, \tag{2}$$

$$\boldsymbol{u}_c \times \boldsymbol{e}_y(y = 0) = \boldsymbol{0}. \tag{3}$$

The subscripts c and d are henceforth used to distinguish between the liquid (continuous) and particle (dispersed) phase, respectively. $\boldsymbol{e}_x$ and $\boldsymbol{e}_y$ are unit vectors pointing in the horizontal and vertical directions, respectively. At the other end of the domain, both phases move with the velocity of the piston,

$$\boldsymbol{u}_d(y = H(t)) = \boldsymbol{u}_c(y = H(t)) = U_h(t)\boldsymbol{e}_x + U_v(t)\boldsymbol{e}_y. \tag{4}$$

Note that $\boldsymbol{u}_d$ and $\boldsymbol{u}_c$ represent the mass averaged interstitial velocities of the phases.

The second situation, i.e., the cross-flow filtration (cf. Figure 1b), differs from the piston driven consolidation in that the piston is replaced by an infinite body of liquid. Next to the filter, at the onset of our experiment, there is a layer of homogeneous suspension with thickness H_0, containing a finite amount of particles. The initial concentration ϕ_0 is assumed lower than the gel value ϕ_g. A drainage flux density $J(t)$ perpendicular to the filter is achieved by maintaining a constant pressure p_∞ in the particle free liquid. Also, a constant flow U_∞ parallel to the plate (in the x-direction) is generated in the bulk of the clear liquid far above the mat. Since the amount of solid phase is limited, all particles will eventually be deposited on the filter. Asymptotically, a situation is reached in which there is a mat of flocculated particles of thickness H_∞ residing on the filter, through which there is a flow of clear liquid. It is this asymptotic situation that will be considered. It shall become clear later that our particular choice of initial particle concentration distribution results in a unique asymptotic solution that can be determined without solving the transient consolidation process. The resistance to flow through the particle structure results in a vertical hydrodynamic load that increases progressively from zero at the top of the mat to a maximum value at the filter. The horizontal bulk flow results in horizontal stresses on the mat. It will later be seen that both phases in the two-phase region move with the same horizontal velocity. If the horizontal velocity at the top of the mat in the asymptotic limit is denoted $U_{h\infty}$, and the corresponding drainage flux J_∞, the shear stress induced by the bulk flow on the suspension in the mat is

$$\Sigma_{h\infty} = -\rho_c J_\infty (U_\infty - U_{h\infty}), \tag{5}$$

where the parameter ρ_c is the density of the continuous phase. It is assumed that $U_{h\infty}/U_\infty \ll 1$, and $U_{h\infty}$ can hence be neglected in Eq. 5.

Balance equations

The following quantities are defined,

$$\boldsymbol{j}_d = \phi \boldsymbol{u}_d, \tag{6}$$

$$\boldsymbol{j}_c = (1 - \phi)\boldsymbol{u}_c, \tag{7}$$

$$\boldsymbol{j} = \boldsymbol{j}_d + \boldsymbol{j}_c, \tag{8}$$

$$\boldsymbol{j}_r = \boldsymbol{j}_d - \phi \boldsymbol{j} = \phi(1 - \phi)(\boldsymbol{u}_d - \boldsymbol{u}_c), \tag{9}$$

where $\boldsymbol{j}_d$ and $\boldsymbol{j}_c$ are the particle and liquid volume flux densities (i.e., the superficial velocities), $\boldsymbol{j}$ is the mixture (or suspension) volume flux density, and $\boldsymbol{j}_r$ is the dispersed phase flux density relative to the mixture.

The requirement of global volume continuity, and continuity of the dispersed phase, read, respectively,

$$\nabla \cdot \boldsymbol{j} = 0, \tag{10}$$

$$\frac{\partial \phi}{\partial t} + \nabla \cdot \boldsymbol{j}_{\mathrm{d}} = 0. \tag{11}$$

Neglecting all effects of inertia, the momentum balance for the suspension mixture can be expressed as (see e.g., Ungarish,[27] p. 22),

$$0 = -\nabla p_{\mathrm{c}} - \nabla \cdot \boldsymbol{\sigma}_{\mathrm{d}} + \nabla \cdot \boldsymbol{\tau}_{\mathrm{Nd}}. \tag{12}$$

Above, $\boldsymbol{\sigma}_{\mathrm{d}}$ is the stress tensor originating from deformation-rate independent inter-particle forces, and $\boldsymbol{\tau}_{\mathrm{Nd}}$ represents rate dependent (viscous) stresses within the particle phase. For simplicity, no such forces have been attributed to the liquid phase, which is justifiable if the viscous liquid stresses are small compared to the components of $\boldsymbol{\tau}_{\mathrm{Nd}}$. The stress tensor $\boldsymbol{\sigma}_{\mathrm{d}}$ can be split into an isotropic "particle pressure", denoted p_{d}, and a deviatoric remainder $\boldsymbol{\tau}_{\mathrm{d}}$, according to

$$-\boldsymbol{\sigma}_{\mathrm{d}} = -p_{\mathrm{d}}\boldsymbol{I} + \boldsymbol{\tau}_{\mathrm{d}}, \tag{13}$$

where $\boldsymbol{I}$ denotes the identity tensor. Traditionally, $\boldsymbol{\tau}_{\mathrm{d}}$ is not included in studies of consolidation. Note that according to Eq. 13 compressive stress components are positive.

The following constitutive relation is adopted for the relative flux density,

$$\boldsymbol{j}_{\mathrm{r}} = -\phi(1-\phi)\frac{k(\phi)}{\mu_{\mathrm{c}}}(\nabla \cdot \boldsymbol{\sigma}_{\mathrm{d}} - \nabla \cdot \boldsymbol{\tau}_{\mathrm{Nd}}). \tag{14}$$

In Eq. 14, μ_{c} is the dynamic viscosity of the liquid phase, and $k(\phi)$ is the permeability of the particle network, for which we take the relation

$$k(\phi) = \frac{1}{3.5 S_0^2 \phi^{1.5}}. \tag{15}$$

It was suggested for low concentration pulp mats by Ingmanson et al.,[28] and the parameter S_0 is the specific surface of the fibres. The postulate Eq. 14 can be derived from a two-fluid description of the suspension in which the exchange of momentum between the phases is accounted for by Darcy's law. To close the system, constitutive relations are needed for $\boldsymbol{\sigma}_{\mathrm{d}}$ and $\boldsymbol{\tau}_{\mathrm{Nd}}$. We shall focus on the rate-independent stresses, and refer to the Appendix for the viscous stresses $\boldsymbol{\tau}_{\mathrm{Nd}}$.

Rate independent solid stresses

Let us assume that the dispersed phase behaves like a plastic-rigid material. Subject to sufficiently small loads, the solid phase resists all deformations. When the local stresses fulfill the following yield criterion, which stems from the modified Cam-clay theory introduced in the field of soil mechanics by Roscoe and Burland,[29] the particle phase will deform irreversibly,

$$F(\boldsymbol{\sigma}_{\mathrm{d}}, \phi) = F(p_{\mathrm{d}}, q_{\mathrm{d}}, p_0(\phi)) = q_{\mathrm{d}}^2 - M^2 p_{\mathrm{d}}(p_0(\phi) - p_{\mathrm{d}}) = 0. \tag{16}$$

Here, q_{d} is (up to a constant factor) the von Mises effective stress used in classical plasticity theory. It is defined as

$$q_{\mathrm{d}} = \sqrt{\tau_{\mathrm{d}}^{ij}\tau_{\mathrm{d}}^{ij}} = \sqrt{(\sigma_{\mathrm{d}}^{ij} - \frac{1}{3}\delta^{ij}\sigma_{\mathrm{d}}^{kk})(\sigma_{\mathrm{d}}^{ij} - \frac{1}{3}\delta^{ij}\sigma_{\mathrm{d}}^{kk})}, \tag{17}$$

δ^{ij} denoting Kronecker's delta. The particle pressure expressed in component form is

$$p_{\mathrm{d}} = \frac{1}{3}\sigma_{\mathrm{d}}^{kk}. \tag{18}$$

Equation 16 describes an elliptic "yield-surface" in $p_{\mathrm{d}} - q_{\mathrm{d}}$ space, centered around $(p_{\mathrm{d}}, q_{\mathrm{d}}) = (p_0(\phi)/2, 0)$, and with a major and minor axis of length $p_0(\phi)$ and $Mp_0(\phi)$, respectively. The ϕ-dependence reveals that we assume the resistance to deformation to be dependent on the local fraction of particles. The function $p_0(\phi)$ expresses the yield limit when purely isotropic loads are applied, and we adopt the relation

$$p_0(\phi) = m(\phi - \phi_{\mathrm{g}})^n, \tag{19}$$

where m and n are positive constants. Equation 19 ensures a strain-hardening behavior, and its form is motivated by previous observations indicating that the yield-limit in uniaxial compression is consistent with power-law behavior.[18]

Whenever $F(\boldsymbol{\sigma}_{\mathrm{d}}, \phi) < 0$, the stress-state lies "inside" the yield-surface, and the dispersed phase behaves locally like a stiff body. In a general situation the stress state in the particle phase would then not be determinate. One way to address this problem is to prescribe an elastic behavior before irreversible deformations occur. We shall however simply assume that, at all instants, the stresses in the solid phase are such that the criterion Eq. 16 is fulfilled. As a consequence, the model will not be able to properly describe situations where the stress-state moves to the inside of the yield-surface (unloading). Below it will become evident that this limitation is not quite as restrictive as it might first seem.

We now adopt an associated flow rule. The flow potential then coincides with the yield surface, and when deformations occur, the components of the strain-rate tensor of the dispersed phase, $\boldsymbol{e}_{\mathrm{d}}$, are obtained as

$$-e_{\mathrm{d}}^{ij} = -\frac{1}{2}\left(\frac{\partial u_{\mathrm{d}}^i}{\partial x^j} + \frac{\partial u_{\mathrm{d}}^j}{\partial x^i}\right) = X\frac{\partial F}{\partial \sigma_{\mathrm{d}}^{ij}}, \quad X \geq 0. \tag{20}$$

Equation 20 implies that the deformation-rate vector (in strain-rate space) is pointing in the direction of the outward normal to the yield surface (a result of the principle of maximum plastic work). The negative sign in front of e_{d}^{ij} ensures that compression corresponds to negative values of $\nabla \cdot \boldsymbol{u}_{\mathrm{d}}$, and the proportionality factor X sets the magnitudes of the components. If the six independent deformation rates e_{d}^{ij} are known, Eqs. 16 and 20 provide us with seven equations for the six independent stresses σ_{d}^{ij} and X. Note that we could not have determined the strain-rates from a known stress state, as Eq. 16 only relates the (then) known stress components. In traditional plasticity theory, where the stresses are provided by elastic constitutive relations, the proportionality factor X is determined by requiring that the stress state remains on the yield-surface during its evolution due to strain-hardening

(the "consistency condition"). The strain-rates can then be obtained.

Let us introduce the volumetric and deviatoric strain rate invariants of the dispersed phase, corresponding to the definitions Eqs. 17 and 18 for the stresses,

$$e_{\mathrm{p}} = e_{\mathrm{d}}^{kk} \quad \text{and} \quad e_{\mathrm{q}} = \sqrt{(e_{\mathrm{d}}^{ij} - \frac{1}{3}\delta^{ij}e_{\mathrm{d}}^{kk})(e_{\mathrm{d}}^{ij} - \frac{1}{3}\delta^{ij}e_{\mathrm{d}}^{kk})}. \quad (21)$$

Using Eqs. 17, 18, and 21 together with Eqs. 16 and 20, we can derive that

$$e_{\mathrm{p}} = -X\frac{\partial F}{\partial p_{\mathrm{d}}} = -2XM^2\left(p_{\mathrm{d}} - \frac{p_0(\phi)}{2}\right), \quad (22)$$

$$e_{\mathrm{q}} = X\frac{\partial F}{\partial q_{\mathrm{d}}} = 2Xq_{\mathrm{d}}. \quad (23)$$

Equations 16, 22, and 23 suffice to obtain p_{d}, q_{d} and X from the deformation rate measures e_{p} and e_{q}. Combining the last two expressions yields the following useful relations for X,

$$X = \frac{e_{\mathrm{q}}}{2q_{\mathrm{d}}} = -\frac{e_{\mathrm{p}}}{2M^2\left(p_{\mathrm{d}} - \frac{p_0(\phi)}{2}\right)} \geq 0. \quad (24)$$

As a consequence of the inequality, compression ($e_{\mathrm{p}} < 0$) takes place for $p_{\mathrm{d}} > p_0(\phi)/2$, and expansion for $p_{\mathrm{d}} < p_0(\phi)/2$. Isochoric deformations can occur only if $p_{\mathrm{d}} = p_0(\phi)/2$, which is referred to as the critical state. Of course, the deviatoric deformation rate can then not be determined by Eq. 24. From the yield surface Eq. 16 and the flow rule Eq. 20, it is possible to obtain an arbitrary deformation-rate component as

$$e_{\mathrm{d}}^{ij} = 2X\left(-\frac{1}{3}M^2\left(p_{\mathrm{d}} - \frac{1}{2}p_0(\phi)\right)\delta^{ij} + \tau_{\mathrm{d}}^{ij}\right). \quad (25)$$

The constitutive theory for $\boldsymbol{\sigma}_{\mathrm{d}}$ will now be applied to the considered consolidation problem.

Analysis

Scaling

As a representative length scale in our problem, we identify in the piston driven case the initial distance between the filter and the piston, and for the cross-flow filtration the thickness of the initial suspension region[†], both denoted H_0. We further let U_0 be the velocity scale, and l a typical size of the pores in the particle network. We shall use $l = 1/S_0$. The magnitude of the rate-independent solid stresses is denoted σ_1. The following scaled variables are defined,

$$\boldsymbol{x}^* = \frac{\boldsymbol{x}}{H_0}, \quad t^* = \frac{U_0 t}{H_0}, \quad \boldsymbol{u}_\alpha^* = \frac{\boldsymbol{u}_\alpha}{U_0}, \quad \boldsymbol{j}_\alpha^* = \frac{\boldsymbol{j}_\alpha^*}{U_0}, \quad \boldsymbol{e}_{\mathrm{d}}^* = \frac{H_0\boldsymbol{e}_{\mathrm{d}}}{U_0}, \quad (26)$$

$$X^* = \frac{H_0\sigma_1 X}{U_0}, \quad p_{\mathrm{c}}^* = \frac{l^2 p_{\mathrm{c}}}{\mu_{\mathrm{c}}U_0H_0}, \quad \boldsymbol{\tau}_{\mathrm{Nd}}^* = \frac{H_0\boldsymbol{\tau}_{\mathrm{Nd}}}{\mu_{\mathrm{d}}U_0}, \quad \boldsymbol{\sigma}_\alpha^* = \frac{\boldsymbol{\sigma}_\alpha}{\sigma_1}, \quad (27)$$

$$K(\phi) = \frac{k(\phi)}{l^2}, \quad P_0(\phi) = \frac{p_0(\phi)}{\sigma_1}, \quad (28)$$

where the superscripts * indicate dimensionless quantities. Above, $\boldsymbol{u}_\alpha$ denotes any of the velocities, $\boldsymbol{j}_\alpha$ represents all the flux densities, and $\boldsymbol{\sigma}_\alpha$ is either $\boldsymbol{\sigma}_{\mathrm{d}}$ or $(\Sigma_v(t), \Sigma_h(t))$. Note that the liquid pressure is scaled with an estimate of the inter-phase drag (assumed given by Darcy's law) accumulated over the distance H_0, and that $\boldsymbol{\tau}_{\mathrm{Nd}}$ is scaled by an expression assuming Newtonian viscous particle stresses, and further that this estimate involves an effective particle phase viscosity μ_{d}.

Inserting the scaled variables into Eqs. 12 and 14, these become, respectively,

$$0 = -\nabla p_{\mathrm{c}} - \frac{1}{Pe}\nabla\cdot\boldsymbol{\sigma}_{\mathrm{d}} + \Lambda\nabla\cdot\boldsymbol{\tau}_{\mathrm{Nd}}, \quad (29)$$

$$\boldsymbol{j}_{\mathrm{r}} = -\phi(1-\phi)K(\phi)\left(\frac{1}{Pe}\nabla\cdot\boldsymbol{\sigma}_{\mathrm{d}} - \Lambda\nabla\cdot\boldsymbol{\tau}_{\mathrm{Nd}}\right), \quad (30)$$

where the superscripts * have been dropped for ease of notation. We shall continue to do so. Two dimensionless groups have appeared, a Péclet number

$$Pe = \frac{\mu_{\mathrm{c}}H_0U_0}{l^2\sigma_1}, \quad \text{and} \quad \Lambda = \frac{\mu_{\mathrm{d}}}{\mu_{\mathrm{c}}}\left(\frac{l}{H_0}\right)^2. \quad (31)$$

Pe expresses the ratio between transport of particles towards the filter by convection, and relative transport away from the filter due to gradients in the inter-particle stresses. Considering that all particles are retained by the filter, these two mechanisms must be equally important in the region next to the filter. Hence, we set $Pe = 1$. Consider now the piston driven filtration. When the piston is controlled by specifying its velocity, we take U_0 as the initial vertical velocity, $U_{\mathrm{v}}(0^+)$, immediately after the consolidation process starts. The definition of Pe then provide the stress measure σ_1,

$$\sigma_1 = \frac{\mu_{\mathrm{c}}H_0U_0}{l^2}. \quad (32)$$

On the other hand, if the process is controlled by the applied loads, we let σ_1 be the initial vertical load, i.e., $\Sigma_{\mathrm{v}}(0^+)$. The velocity scale is then

$$U_0 = \frac{l^2\sigma_1}{\mu_{\mathrm{c}}H_0}. \quad (33)$$

The group Λ measures the significance of the viscous stresses. Since l/H_0 is small, these are only important to the momentum balance of the mixture if $\mu_{\mathrm{d}}/\mu_{\mathrm{c}} \gg 1$. As shall become clear below, even small rate-dependent stresses can nevertheless have an influence on the behavior of the flow field. Further, in regions where the solid phase network reaches critical state, the applied load must necessarily be balanced by rate-dependent stresses, as the then isochoric deformations do not result in strain-hardening.

In the cross-filtration case, we shall use $\sigma_1 = p_\infty$, and obtain U_0 from Eq. 33. The nondimensional form of Eq. 5 then becomes,

$$\sum\nolimits_{\mathrm{h}\infty} = -Re_\infty\left(\frac{l}{H_0}\right)^2 J_\infty, \quad \text{where} \quad Re_\infty = \frac{\rho_{\mathrm{c}}U_\infty H_0}{\mu_{\mathrm{c}}}. \quad (34)$$

[†]Taking the asymptotic thickness of the particle mat as the length scale would be more physically relevant, but to control this parameter is more difficult than to control H_0 (or, rather, to control the total quantity of particles ϕ_0H_0).

Apart from Eqs. 5, 12, and 14, the relations retain their appearances when scaled variables are introduced, except that $p_0(\phi)$ should be replaced by $P_0(\phi)$ at all occurrences. From now on, we shall only refer to scaled quantities, unless otherwise explicitly specified.

Sheared consolidation

Assume a situation of plane strain in the xy-plane. Because of the infinite dimensions of the domain, we suppose that there are no horizontal gradients. Hence, from Eq. 10, the mixture flux towards the filter, j^y, is the same at all vertical positions. In the piston driven and the cross-flow cases we have, respectively,

$$j^y = U_v(t) \quad \text{and} \quad j^y = J(t). \tag{35}$$

The horizontal and vertical components of the force balance Eq. 29 can be integrated to reveal, respectively,

$$\tau_d^{xy} + \Lambda\tau_{Nd}^{xy} = \Sigma_h(t), \tag{36}$$

$$p_c + \sigma_d^{yy} - \Lambda\tau_{Nd}^{yy} = \Sigma_v(t), \tag{37}$$

indicating how the applied load is distributed between different types of stresses. During the cross-flow filtration, the vertical load equals the liquid pressure, so that $\Sigma_v(t) = 1$. From Eqs. 30, 36, and 37, we obtain the relative flux density components,

$$j_r^x = 0 \tag{38}$$

$$j_r^y = -\phi(1-\phi)K(\phi)\frac{\partial}{\partial\phi}(\sigma_d^{yy} - \Lambda\tau_{Nd}^{yy}). \tag{39}$$

Consequently, both phases have the same velocity in the horizontal direction.

From our assumptions about the deformations, we have $e_d^{xx} = e_d^{zz} = e_d^{xz} = e_d^{yz} = 0$. It follows from Eq. 25 that

$$\tau_d^{xx} = \tau_d^{zz} = -\frac{1}{2}\tau_d^{yy} = \frac{1}{3}M^2\left(p_d - \frac{1}{2}P_0(\phi)\right), \quad \tau_d^{xz} = \tau_d^{yz} = 0. \tag{40}$$

Above, we have made use of the fact that $\tau_d^{kk} = 0$. For the nonzero strain rates we obtain

$$e_d^{xy} = 2X\tau_d^{xy}, \quad e_d^{yy} = -2XM^2(p_d - \frac{1}{2}P_0(\phi)). \tag{41}$$

The assumption made previously that the stress state always fulfils the yield criterion provides us with a relation between $\sigma_d^{yy} = p_d - \tau_d^{yy}$ and τ_d^{xy}. Using the results Eq. 40, the yield surface can be written as

$$\frac{\left(\sigma_d^{yy} - \frac{1}{2}P_0(\phi)\right)^2}{\left(\frac{1}{2}P_0(\phi)\sqrt{1+\frac{2}{3}M^2}\right)^2} + \frac{\tau_d^{xy^2}}{\left(\frac{1}{2}P_0(\phi)\frac{M}{\sqrt{2}}\right)^2} = 1. \tag{42}$$

This is an ellipse in the plane $(\sigma_d^{yy}, \tau_d^{xy})$, centered at $(P_0(\phi)/2,0)$, and with a major and minor axis of length $P_0(\phi)\sqrt{1+\frac{2}{3}M^2}$ and $P_0(\phi)\frac{M}{\sqrt{2}}$, respectively (see Figure 2)[‡]. The top of the yield-ellipse always remains on the dashed straight line in the figure, when it expands or contracts due to changes in the concentration. If the particle phase is not subject to any horizontal shear stresses, the yield-limit is given by the intersection of the ellipse and the horizontal axis. Observe that the stress states on the ellipse of Figure 2 in the plane $(\sigma_d^{yy}, \tau_d^{xy})$ correspond only to part of the stress states defined by the original yield surface in the (p_d, q_d)-plane given by Eq. 16, since here we allow only a particular class of deformations as previously described. As a result of this, and the change of variables from (p_d, q_d) to $(\sigma_d^{yy}, \tau_d^{xy})$, the ellipse in Figure 2 has a different appearance than the original yield surface. In particular, the stress state of the origin in the (p_d, q_d)- plane is not a part of the yield surface in Figure 2 since that would correspond to an isotropic expansion, a deformation excluded in our formulation.

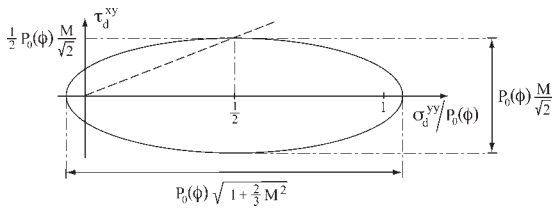

Figure 2. The yield-surface in the $\sigma_d^{yy} - \tau_d^{xy}$-plane.

The dashed line indicates the position of the critical stress state at different concentrations.

As the flow rule Eq. 20 tells us that the deformation-rate of the solid phase is perpendicular to the yield-surface, we can also relate the horizontal and vertical directions in Figure 2 with compression in the y-direction and shearing in the x-direction, respectively. Consequently, $\sigma_d^{yy} = P_0(\phi)/2$ separates the possible stress states into two halves, such that when σ_d^{yy} is larger (smaller) than $P_0(\phi)/2$, yielding of the particle phase will result in compression (expansion). This particular value of σ_d^{yy} will be denoted $\sigma_c(\phi)$, and the corresponding value of τ_d^{xy} is $\tau_c(\phi)$. Thus, at the stress state

$$(\sigma_c(\phi), \tau_c(\phi)) = \left(\frac{P_0(\phi)}{2}, \frac{MP_0(\phi)}{2\sqrt{2}}\right), \tag{43}$$

shearing of the solid phase obviously occurs without volumetric deformations, which hence corresponds to the critical state, and the dashed line in Figure 2 is accordingly referred to as the "critical state line." If the flocculated structure expands, the particle concentration decreases and the dispersed phase becomes weaker (the yield-surface shrinks). In these situations, and at the critical state, rate-dependent stresses or inertia are needed to determine the deformation rates as strain-hardening fails to do so.

The cross-flow filtration asymptotic limit

We now proceed to consider the asymptotic limit of the cross-flow filtration case. The vertical displacement of particles has then ceased, and, as $u_d^y = 0$ everywhere, there is no normal viscous stress τ_{Nd}^{yy} in the flocculated network (cf. the Appendix). Vertical load is transferred from the liquid to the dispersed phase through inter-phase drag. Consequently, the vertical stress σ_d^{yy} will increase progressively, from $\sigma_d^{yy} = 0$ at $y = H_\infty$, to $\sigma_d^{yy} = 1$ at the filter, where $p_c = 0$. Given our assumption about an initially nonconsolidated suspension $(\phi_0 < \phi_g)$, the stress states at all positions in the consoli-

[‡]No deformations take place in the principal stress direction z. Thus, due to the associated flow rule, the yield-ellipse Eq. 42 is a line on the surface of the yield-ellipsoid in principal stress space, such that the normal to the surface along the line has no component in the z-direction.

dated mat are located on the yield surfaces corresponding to the local volume fraction of particles. This would not necessarily be true if a consolidated mat existed already at the onset of the cross-flow filtration process, in which case parts (or the whole) of the mat might be of sufficient strength to withstand the applied loads, and the yield criterion would not be everywhere fulfilled. In general, the solution for the asymptotic limit depends on both the initial particle fraction distribution and the way the loads are brought to their final values (cf. Johnson and Jackson[22]). In the situation under consideration, depending on the magnitude of the horizontal load, one of three qualitatively different situations is obtained as illustrated in Figure 3.

The top sub-figure illustrates the situation without horizontal load. In the asymptotic limit, the entire mat is then stagnant. By definition, the yield-surfaces associated with the solid phase at various positions must pass through the rate-independent stress-states $(\sigma_d^{yy}, \tau_d^{xy})$ at these positions. Hence, as $\tau_d^{xy} = 0$ in the absence of a shear load, the stress states in the mat are located along the σ_d^{yy}-axis on the series of yield surfaces representing the strength of the mat at its local particle concentration. These states are indicated by the thick line in the figure.

The middle sub-figure corresponds to a situation with a shear load such that $(1, \Sigma_{h\infty})$ is located on the compression side of the critical state line in $\sigma_d^{yy} - \tau_d^{xy}$-space. The particle concentration at $y = 0$ is thus determined by the requirement that the yield surface passes through the applied load $(1, \Sigma_{h\infty})$. Further into the mat (i.e., for larger y), the vertical load transmitted to the solid phase and the local particle concentration are smaller. The yield surfaces must therefore there pass through $(\sigma_d^{yy}(y), \Sigma_{h\infty})$, where $\sigma_d^{yy}(y)$ and $\phi(y)$ are decreasing functions of y. This corresponds to moving along the horizontal thick line in the figure. The rate independent stress states thus creep towards the top of the yield-ellipses as y increases until, at $y = y_1$, critical state is reached. The corresponding concentration is denoted ϕ_1. Up to this position, the rate independent stresses have been able to balance the applied load, and $0 \le y \le y_1$ is a stagnant region where no deformations occur. At positions further away from the filter $(y > y_1)$, the solid phase is at critical state and

$$\sigma_d^{yy}(y) = \sigma_c(\phi(y)), \tag{44}$$

$$\tau_d^{xy}(y) = \tau_c(\phi(y)). \tag{45}$$

In this region, the rate independent stresses are unable to balance the applied load alone (note that no yield surface corresponding to a vertical stress $\sigma_d^{yy} < \sigma_c(\phi_1)$ passes through $(\sigma_d^{yy}, \Sigma_{h\infty})$ as this would represent an unstable state where any small disturbance would lead to expansion and weakening of the particle phase). The rate independent stress states given by Eqs. 44 and 45 correspond to the intersection between the yield-surfaces and the critical state line. These intersections are located along the slanted thick line. In this region, as prescribed by Eq. 36, the viscous stress τ_{Nd}^{xy} balances the difference between $\Sigma_{h\infty}$ and the maximum rate-independent shear stress $\tau_d^{xy} = \tau_c(\phi)$ that can be carried by the solid phase without deforming. As ϕ varies, so will the viscous stress τ_{Nd}^{xy}.

The last of the sub-figures corresponds to a situation in which $(1, \Sigma_{h\infty})$ is located on the expansion side of the critical state line. The entire mat is then in the same state of shear flow as the region $y > y_1$ above, i.e., in this scenario $y_1 = 0$. We proceed under the assumption that $\Sigma_{h\infty} \neq 0$ and that y_1 is finite, knowing that if this is not the case, only minor adjustments of the analysis need to be made, as commented upon below.

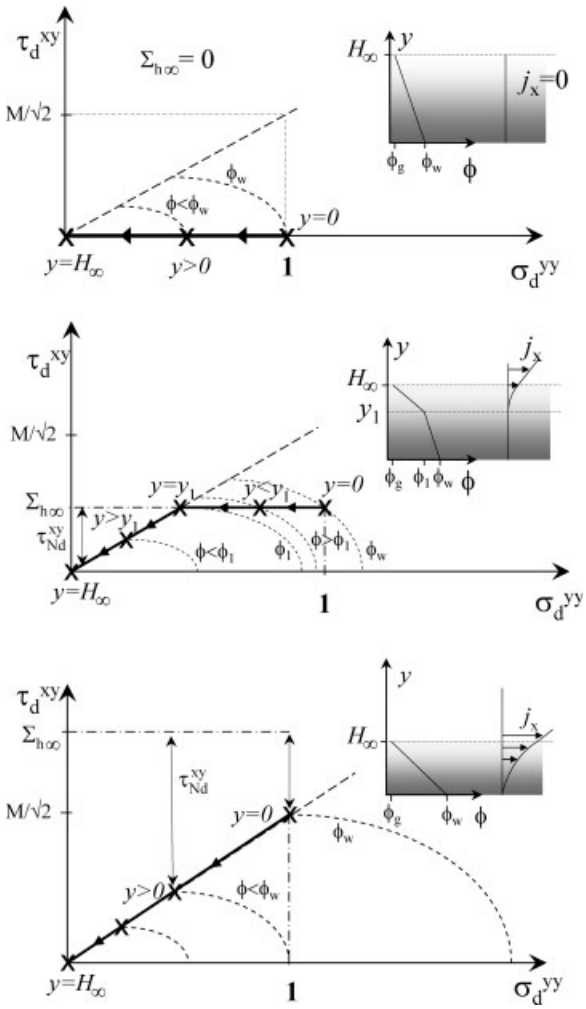

Figure 3. Yield surfaces (in nondimensional units) at different vertical positions in the asymptotic mat for different shear loads.

The straight line through the origin indicates the position of the critical stress states. ϕ_w and ϕ_1 are the concentrations at the filter and at the position separating the stagnant and the continuously deforming regions, respectively. Top figure: $\Sigma_{h\infty} = 0$. Middle figure: $\Sigma_{h\infty} < M/\sqrt{2}$. Bottom figure: $\Sigma_{h\infty} > M/\sqrt{2}$. The rate-independent stresses at different positions are given by the bold lines, with arrows indicating the direction of increasing y. For some of these states part of the corresponding yield surfaces are given by the dashed curved lines. The small diagrams qualitatively outline the concentration and horizontal flux profiles.

Since the network is uncompressed at $y = H_\infty$, the network has zero strength at that position, and

$$\phi(y = H_\infty) = \phi_g. \tag{46}$$

It follows from equation Eq. 36 that the shear load $\Sigma_{h\infty}$ must then be completely balanced by the viscous stress τ_{Nd}^{xy}.

Further towards the filter, the particle network will be increasingly more compressed, and the yield surfaces of finite size. An increasing fraction of $\Sigma_{h\infty}$ will therefore be balanced by the solid stress component τ_d^{xy}, and less by the viscous stress τ_{Nd}^{xy}. At $y = y_1$, the system is at critical state, but all load is carried by the rate-independent stress. The concentration ϕ_1 at this point can be determined from the relation

$$\left[\tau_d^{xy} = \tau_c(\phi_1) = \Sigma_{h\infty}\right]_{y=y_1}. \tag{47}$$

Limiting the treatment to compressive stress states, the yield surface Eq. 42 can be turned into a relation for σ_d^{yy},

$$\sigma_d^{yy}(y) = f(\phi(y), \tau_d^{xy}(y)). \tag{48}$$

Equation 48 may, at least when $P_0(\phi)$ is given by Eq. 19, be inverted with respect to ϕ. By inserting the normal solid stress at the surface of the filter, as well as $\tau_d^{xy} = \Sigma_{h\infty}$, the concentration at the filter is found to be

$$\phi(y = 0) = \phi_w = f_\phi^{-1}(1, \Sigma_{h\infty}), \tag{49}$$

the subscript ϕ indicating the variable with respect to which the inversion is performed.

As the vertical velocity of the dispersed phase is zero, it follows from the definitions Eqs. 6 and 9 that $\mathbf{j}_r^y = -\phi\,\mathbf{j}^y$. Using Eqs. 35 and 39, we then derive

$$J_\infty = (1-\phi)K(\phi)\frac{\partial \sigma_d^{yy}}{\partial y}, \tag{50}$$

where J_∞ is the asymptotic limit of the drainage flux density $J(t)$. The stress σ_d^{yy} is uniquely determined by $\phi(y)$, albeit through different relations in the upper and lower parts of the mat. Consider first the region $0 \le y \le y_1$. Inserting Eq. 48 into Eq. 50, a separable differential equation is obtained, which when integrated from $y = 0$ to a position $y \le y_1$ turns into

$$yJ_\infty = \int_{\phi_w}^{\phi(y)} (1-\phi')K(\phi')\frac{df(\phi';\sum_{h\infty})}{d\phi'}d\phi' \quad 0 \le y \le y_1. \tag{51}$$

The load $\Sigma_{h\infty}$ is regarded as a parameter. Provided J_∞ is known, Eq. 51 permits us to determine $\phi(y)$ at any position in the stagnant part of the mat. Specifically, if Eq. 51 is evaluated at $y = y_1$, where $\phi = \phi_1$ is calculated using Eq. 47, we obtain an equation for the location of the boundary between the shear-flow and the stagnant domains.

The upper part of the mat is treated in an analogous fashion. The normal solid stress is now given by Eq. 44, and we find by integrating the separable differential equation from $y = y_1$ that

$$(y-y_1)J_\infty = \int_{\phi_1}^{\phi(y)} (1-\phi')K(\phi')\frac{d\sigma_c(\phi')}{d\phi'}d\phi' \quad y_1 \le y \le H_\infty. \tag{52}$$

Equation 52 yields the concentration in the shear-flow region, again provided J_∞ is known. Evaluating the equation at $y = H_\infty$, where $\phi = \phi_g$, an equation is obtained for the thickness of the mat.

The drainage flux density J_∞ is determined from the requirement that the total quantity of solid phase is conserved, i.e.

$$\phi_0 = \int_0^{H_\infty} \phi dy = \int_{\phi_w}^{\phi_g} \phi' \left(\frac{d\phi'}{dy}\right)^{-1} d\phi'. \tag{53}$$

The inverse of the concentration gradient can be obtained in the upper and lower part of the mat by inserting, respectively, Eqs. 44 and 48 into Eq. 50. Employing the results in Eq. 53, the drainage flux is obtained,

$$J_\infty = \frac{1}{\phi_0}\left(\int_{\phi_w}^{\phi_1} \phi'(1-\phi')K(\phi')\frac{df(\phi';\sum_{h\infty})}{d\phi'}d\phi' + \int_{\phi_1}^{\phi_g} \phi'(1-\phi')K(\phi')\frac{d\sigma_c(\phi')}{d\phi'}d\phi'\right). \tag{54}$$

In the special case when $\Sigma_{h\infty} = 0$, there is no deforming region, and the entire mat is treated as the domain $y \le y_1$.

We now consider what changes need to be made to the analysis when $\Sigma_{h\infty} \ge M/\sqrt{2}$. The shear-flow region then extends over the entire mat, i.e., $y_1 = 0$. In the particular case $\Sigma_{h\infty} = M/\sqrt{2}$, the loads on the particle network are just of the right strength to bring the stress state $(\sigma_d^{yy}, \tau_d^{xy})$ at the filter surface to the critical state. Although the flocculated structure is then at critical state at $y = 0$, the rate-independent network stresses there completely balance the transmitted load, and the viscous stress τ_{Nd}^{xy} is zero. Therefore, Eq. 49 can still be used to obtain $\phi_w = \phi_1$. At larger values of $\Sigma_{h\infty}$, the concentration $\phi_w = \phi_1$ must instead be obtained from the condition $\sigma_c(\phi_w) = 1$. Apart from this, the analysis proceeds as described earlier for the shear-flow region.

When the concentration profile $\phi(y)$ has been determined, it is straightforward to calculate the viscous stress $\tau_{Nd}^{xy} = \Sigma_{h\infty} - \tau_c(\phi(y))$ in the region $y_1 \le y \le H_\infty$. The velocity profile $u_d^x(y)$ is then readily obtained, the result depending on the chosen constitutive model for the rate-dependent stresses. It is worth pointing out that the solution for the concentration is the same for all loads $\Sigma_{h\infty} \ge M/\sqrt{2}$. The viscous stress τ_{Nd}^{xy} will however change, and, by consequence, the velocity profile. We have in the analysis assumed that $\Sigma_{h\infty}$ is given *a priori*. The horizontal bulk velocity required to generate the shear load can be calculated *a posteriori* from Eq. 34 once J_∞ has been determined.

The piston driven filtration

To guide the reader through the analysis of the piston driven filtration, Figure 4 qualitatively illustrates the evolution of the volume fraction of solids between the plates, the yield surfaces, and the horizontal flux profiles, when the constant load $(1, \Sigma_h)$ is suddenly applied at $t = 0^+$ in a situation without viscous stresses. Initially, the concentration is homogeneous ϕ_0 and all parts of the suspension are described by the same yield surface. It is assumed that $\Sigma_h < \tau_c(\phi_0)$ in order to avoid that any part of the network reaches critical state. When the load is applied, the concentration immediately rises to ϕ_w at the filter (cf. Eq. 59), which also corresponds to an instantaneous enlargement of the yield surface

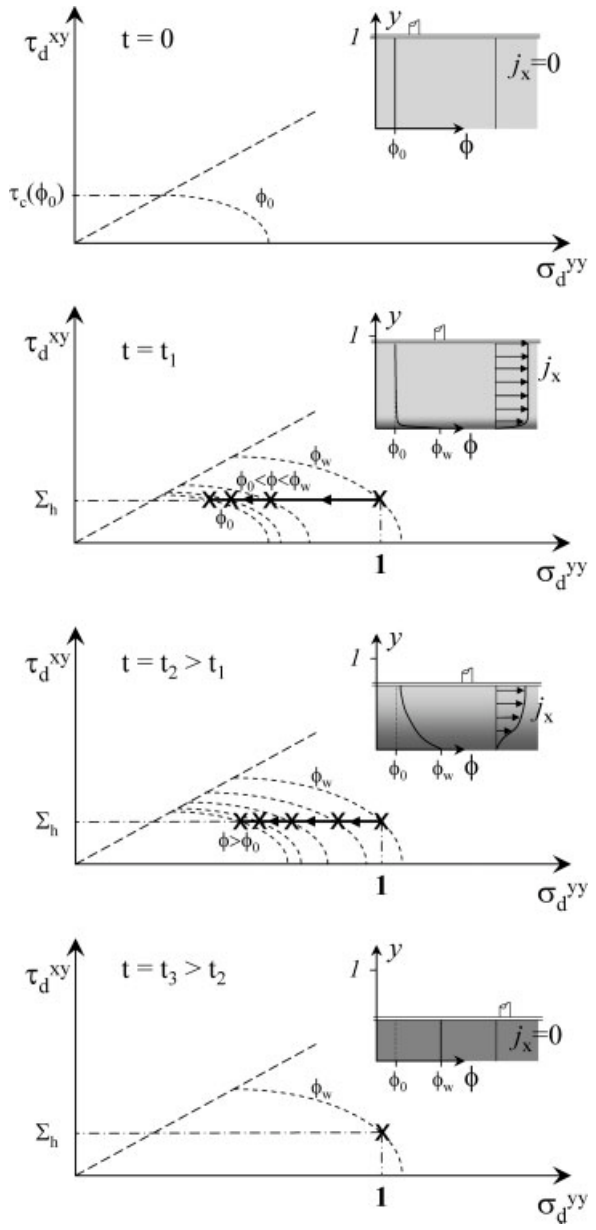

Figure 4. Qualitative yield surfaces at different vertical positions and different instants of time for the piston driven filtration when a constant load (1, Σ_h) is suddenly applied at $t = 0^+$.

The small diagrams qualitatively outline the concentration and horizontal flux profiles. Cf. also the caption of Figure 3.

at that position. The upper part of the network is unaffected, and the yield surfaces are unchanged. This part of the network translates horizontally as a stiff cake. Progressively, the consolidation will spread to the remaining parts of the network with corresponding enlargements of the yield surfaces, until eventually the concentration has become homogeneous and equal to ϕ_w. All parts of the network are then described by the same yield surface again.

A transport equation for the dispersed phase is obtained by inserting the relation between $\boldsymbol{j}_d$ and $\boldsymbol{j}_r$, obtained from Eq. 9, into Eq. 11, and employing the global conservation of volume Eq. 10. If Eq. 35 is then used in this equation, we find

$$\frac{\partial \phi}{\partial t} + U_v(t)\frac{\partial \phi}{\partial y} + \frac{\partial j_r^y}{\partial y} = 0. \tag{55}$$

The viscous stresses will be neglected in the following analysis, i.e., we set $\Lambda = 0$. This is consistent with the hypothesis made by Buscall and White[7] that the deformation of the solid phase is rate-determined by the resistance to displace the two phases with respect to each other, rather than by the resistance to relative movements between particles. It has since been employed in several studies, see, e.g., Howells et al.[9] and Landman et al.[10] The corresponding (more complex) treatment of the viscous case is provided in the Appendix.

To avoid situations where viscous stresses are needed, we assume that the stress-states at all positions, and at all times, are such that $\sigma_d^{yy} > \sigma_c(\phi)$, i.e., on the compressive half of the yield-surface in Figure 2. Equation 48 can then be employed.

Eliminating X from the expressions in Eq. 41, and introducing σ_d^{yy}, we can relate the deformation rates for a given stress state,

$$e_d^{xy} = -\frac{(1+\frac{2}{3}M^2)}{M^2}\frac{\tau_d^{xy}}{(\sigma_d^{yy} - \frac{1}{2}P_0(\phi))}e_d^{yy}. \tag{56}$$

Equations 48 and 56 provide the necessary constitutive coupling between stresses and nonzero deformation rates in the flocculated phase.

By combining the results Eqs. 36, 39, 55, and 48, we find an equation for the concentration,

$$\frac{\partial \phi}{\partial t} + U_v(t)\frac{\partial \phi}{\partial y} = \frac{\partial}{\partial y}\left(D(\phi, \Sigma_h(t))\frac{\partial \phi}{\partial y}\right), \tag{57}$$

where the "diffusivity function" is

$$D(\phi, \Sigma_h(t)) = \phi(1-\phi)K(\phi)\frac{\partial f}{\partial \phi}(\phi, \Sigma_h(t)). \tag{58}$$

The advection-diffusion equation Eq. 57[§] has the same appearance as its counterparts in studies of uniaxial pressure filtration (see, e.g., Landman et al.[10]). The difference is that generalizing the yield-stress concept to include the shear-strength of the flocculated network has introduced an explicit time-dependence in the diffusivity function. As $\Sigma_h(t)$ can be controlled externally, we have some influence over the diffusivity.

The boundary conditions needed to solve Eq. 57 are different depending on whether we control the piston by the applied load, or by prescribing its displacement velocity. Assume first the former alternative, Eqs. 1 and 37 then imply that $\sigma_d^{yy}(0,t)$ is known. So is τ_d^{xy} from Eq. 36, and thus Eq. 48 implicitly provides the volume fraction of particles at the filter,

$$\phi(0,t) = f_\phi^{-1}(\Sigma_v(t), \Sigma_h(t)). \tag{59}$$

[§]Note that for all $\phi \le \phi_g$, $\sigma_d^{yy} \equiv 0$, resulting in $D \equiv 0$. Equation 57 is then of hyperbolic type. However, this is of no concern to us, since we have assumed the suspension to be completely flocculated.

According to Eq. 4, the relative flux is zero at the piston, which through Eq. 39 translates into

$$\frac{\partial \sigma_{\mathrm{d}}^{yy}}{\partial y}(H(t),t) = \frac{\partial \phi}{\partial y}(H(t),t) = 0. \tag{60}$$

Using Eqs. 2 and 35 in the definition Eq. 9, we get the vertical relative flux at the filter in terms of $U_{\mathrm{v}}(t)$ and $\phi(0,t)$. The vertical piston velocity is obtained by combining this result with Eq. 39,

$$U_{\mathrm{v}}(t) = \left[(1-\phi)K(\phi)\frac{\partial \sigma_{\mathrm{d}}^{yy}}{\partial y}\right]_{y=0} = \left[\frac{D(\phi,\sum_{\mathrm{h}}(t))}{\phi}\frac{\partial \phi}{\partial y}\right]_{y=0}. \tag{61}$$

The vertical velocity component is apparently influenced by the applied horizontal shear stress.

To obtain the horizontal velocity of the piston, we first need the deformation rates of the network. Using Eqs. 36 and 48 to eliminate the network stresses in Eq. 56 yields,

$$e_{\mathrm{d}}^{xy} = -g(\phi,\Sigma_{\mathrm{h}}(t))e_{\mathrm{d}}^{yy}. \tag{62}$$

The deformation rates are related to the flux densities as

$$e_{\mathrm{d}}^{xy} = \frac{1}{2}\frac{\partial j^x}{\partial y}, \quad e_{\mathrm{d}}^{yy} = \frac{\partial}{\partial y}\left(\frac{j_{\mathrm{r}}^y}{\phi}\right). \tag{63}$$

The relative flux density in the relation for e_{d}^{yy} can be rewritten as an expression containing $D(\phi,\Sigma_{\mathrm{h}}(t))$ and the gradient of ϕ using Eqs. 39, 48, and 58. Then, insertion of the deformation rates into Eq. 62, followed by integration, yields the horizontal mixture flux density

$$j^x(y,t) = 2\int_0^y g(\phi,\Sigma_{\mathrm{h}}(t))\frac{\partial}{\partial y'}\left(\frac{D(\phi,\sum_{\mathrm{h}}(t))}{\phi}\frac{\partial \phi}{\partial y'}\right)\mathrm{d}y', \tag{64}$$

where the condition $j^x(0,t) = 0$ has been introduced. As $j_{\mathrm{r}}^x = 0$, it follows that $u_{\mathrm{d}}^x = u_{\mathrm{c}}^x = j^x$, and the desired velocity component is $U_{\mathrm{h}}(t) = j^x(H(t),t)$.

When the piston velocity is set, Eq. 60 is still used as a boundary condition. By rewriting Eq. 61, a condition for the concentration gradient at $y = 0$ is obtained, that replaces Eq. 59. The shear stress appearing in the equations is obtained by solving Eq. 64, evaluated at $y = H(t)$, for $\Sigma_{\mathrm{h}}(t)$ as a function of $U_{\mathrm{h}}(t)$.

Finally, if we decide to specify $\Sigma_{\mathrm{v}}(t)$ and $U_{\mathrm{h}}(t)$, we use Eqs. 59–61, but determine $\Sigma_{\mathrm{h}}(t)$ from $U_{\mathrm{h}}(t)$ in the manner just described.

Equations 57–64 have been solved numerically. To facilitate the numerical treatment, a change of coordinates, $y = H(t)\tilde{y}$, was undertaken in order to have a domain with fixed boundaries, $\tilde{y} \in [0,1]$. The spatial discretization was then performed using the Galerkin formulation of the finite element method with linear interpolation functions. For the time-derivative, the implicit Crank–Nicolson formulation was employed. The complete discretization is thus of second order accuracy in both space and time. The implementation of the algorithm was carried out by formulating the problem in variational form, and then using the package femLego for automated code generation.[30]

A shooting method based on Eq. 64 was used to obtain $\Sigma_{\mathrm{h}}(t)$ when $U_{\mathrm{h}}(t)$ was specified. For each time-step, the Eqs. 57–61 were solved using a guessed value for $\Sigma_{\mathrm{h}}(t)$, which was updated till the correct value of $U_{\mathrm{h}}(t)$ was found.

To produce the presented computational results, the domain $\tilde{y} \in [0,1]$ was resolved with 400 elements of uniform size. The nondimensional time step Δt was 3.1×10^{-7}.

Results

For the parameters in Eq. 19 determining the isotropic yield limit, and the specific surface, we chose the values used by Zahrai et al.,[31] i.e., $m = 500$ kPa, $n = 2.5$, and $S_0 = l^{-1} = 18 \times 10^5$ m^{-1}. Buscall et al.[17] conclude that the yield stress in shear for a strongly flocculated polystyrene latex suspension appears to be one to two orders of magnitude smaller than the corresponding uniaxial limit, and Buscall and White[7] argue that this is reasonable, since in shear a substantially larger fraction of the network bonds are in a state of tension. Consequently, M was set to the value 0.287, giving a critical shear stress $\tau_{\mathrm{c}}(\phi)$ that is a fraction 0.1 of the yield limit in uniaxial compression. The viscosity of the continuous phase was $\mu_{\mathrm{c}} = 10^{-3}$ Pas. In all the presented results, the stress scale σ_1 was 1 kPa (i.e., $\Sigma_{\mathrm{v}}(t)$ or p_∞ was 1 kPa), and $H_0 = 0.01$ m. Thus, according to Eq. 33, the velocity scale is $U_0 = 1/324 \times 10^{-2}$ m/s, and the time-scale is $H_0/U_0 = 324$ s. In the cross-flow filtration case, $\phi_0 = 0.005$ and $\phi_{\mathrm{g}} = 0.01$, whereas for the piston driven filtration the corresponding values were $\phi_0 = 0.05$ and $\phi_{\mathrm{g}} = 0$. The latter choice of gel concentration was motivated by simplicity since, by assumption, $\phi_0 > \phi_{\mathrm{g}}$.

Cross-flow filtration

Concentration profiles corresponding to four different shear loads are plotted in Figure 5. When the horizontal load $\Sigma_{\mathrm{h}\infty} < M/\sqrt{2}$, there is a stagnant region adjacent to the filter, in which the particle stresses balances the applied load without the network continuously deforming. The kinks on the curves mark the boundary between the stagnant lower part of the

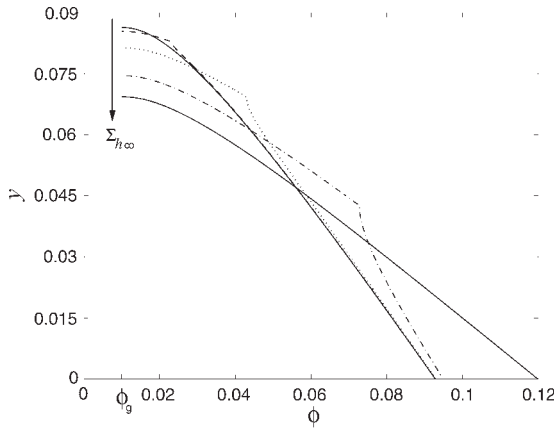

Figure 5. Asymptotic concentration profiles for the cases $\Sigma_{\mathrm{h}\infty} = 0, 10^{-3}, 10^{-2}, 5 \times 10^{-2}$ and $\geq M/\sqrt{2}$.

The kinks on the curves for $\Sigma_{\mathrm{h}\infty} = 10^{-3}, 10^{-2}, 5 \times 10^{-2}$ occur at $y = y_1$. $m/p_\infty = 500$, $n = 2.5$, $M = 0.287$, $\phi_0 = 0.005$, $\phi_g = 0.01$.

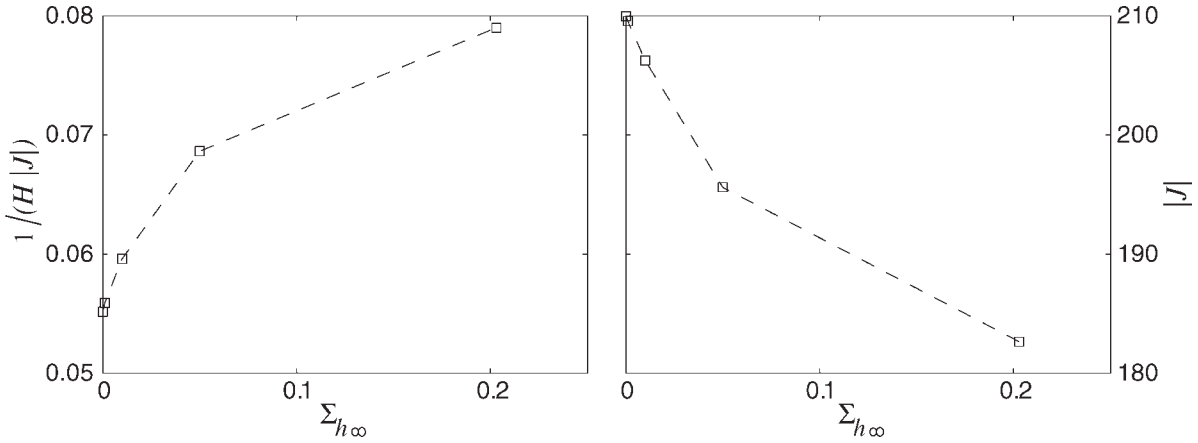

Figure 6. Drainage resistance coefficient (left subfigure) and drainage flux (right subfigure) as functions of the shear load for the cases in Figure 5.

Cf. the caption of that figure for parameter values.

mat, and the shear-flow region on top. At higher shear loads, the network gets more compacted and the stagnant region progressively thinner, until, at the load $\Sigma_{h\infty} = M/\sqrt{2}$, it only just fails to appear. The entire suspension mat is then flowing. Increasing $\Sigma_{h\infty}$ even further does not change the solution for the particle concentration, although the shear rates in the suspension will naturally become larger.

Paradis et al.[32] measure the evolution of the drainage resistance of a fiber sheet, as it is formed under constant drainage pressure and a hydrodynamically applied shear load. The drainage resistance coefficient is defined as the drainage pressure divided by the product of the drainage flux and the instantaneous mat thickness. They find that increasing the shear load results in an increased drainage resistance coefficient for a given surface density of the formed sheet. In the scaled variables employed in the present study, their nondimensional drainage coefficient corresponds to $1/(H|J|)$. This quantity is plotted in Figure 6 as a function of the shear load for the same cases as in Figure 5, together with the magnitude of the drainage flux. The same trend regarding the influence of the shear on the resistance coefficient is seen as was observed by Paradis et al.[32] One should bear in mind, however, that their measurements were obtained during the transient stage of a drainage process, whereas our results stem from a steady state asymptotic analysis.

Piston driven filtration

In the presented calculations, the initial horizontal load was set to zero, while the vertical load was given the value required to precisely balance the stresses in the solid phase at the onset of the consolidation process. At $t = 0$ the piston was thus still. In the purely plastic simulations, the vertical load Σ_v was then instantly raised at $t = 0^+$ to a higher value, and then kept constant, while simultaneously $U_h(t)$ was suddenly increased to a constant value. If viscosity is included, the same procedure would yield very different velocity profiles at small times, as compared to the inviscid case (cf. an impulsively started plane Couette flow for which inertia is neglected). Instead, for reasons explained in the Appendix, the horizontal piston velocity was ramped linearly over a very short time interval to the desired value U_h, after which it was kept constant.

Figure 7 illustrates the evolution of the gap size $H(t)$ for several inviscid cases and one viscous simulation in which $\Lambda = 5.6 \times 10^{-3}$. For reference to dimensional units, using the example of dimensional scales from the beginning of the Results section, one finds that U_h corresponds to a dimensional velocity of 0.01 m/s and that the graph in Figure 7 covers a time interval of about 18 s. The shear loads $\Sigma_h(t)$ required to achieve the chosen values of U_h are shown in Figure 8. It is evident from Figure 7 that the consolidation rate is increased when a shear load is applied. We note that combining a constant vertical load with a constant horizontal piston velocity will eventually result in a situation of pure shear deformation when the compression of the network stops and Σ_v is balanced by the particle stresses. It is a consequence of the associated flow rule that the critical state $(\sigma_c(\phi), \tau_c(\phi))$ has then been reached at all points between the plates. When the drainage ceases, the liquid pressure is

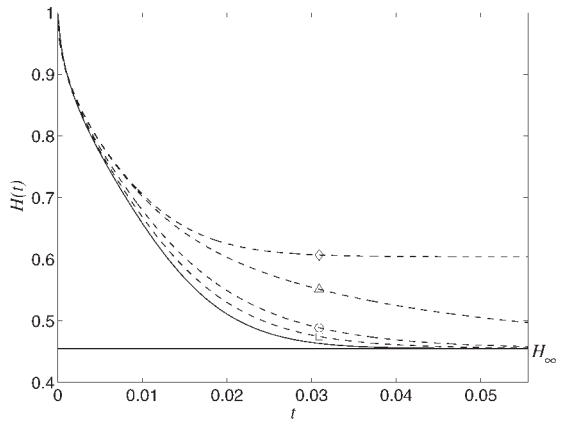

Figure 7. A comparison between different cases of the evolution of the gap *H*(*t*).

In all simulations $\Sigma_v(t) = 1$. Dashed lines: Purely plastic cases. ◇: $U_h = 0$, △: $U_h = 32.4$, ○: $U_h = 162$, □: $U_h = 324$. Solid line: Visco-plastic calculation (only $\tau_{Nd}^{xy} \neq 0$), $U_h = 3240$, $\Lambda = 5.6 \times 10^{-3}$. The horizontal line $H = H_\infty$ corresponds to the asymptotic gap size when $U_h \neq 0$.

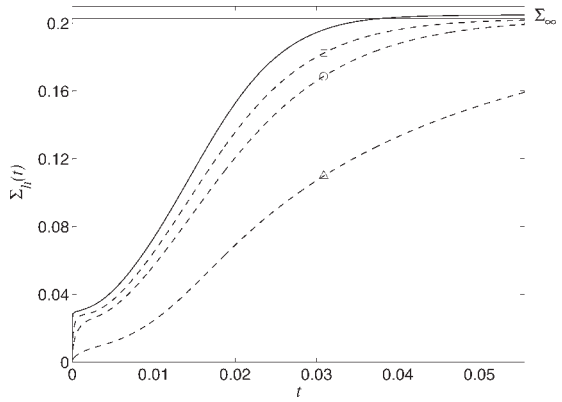

Figure 8. A comparison between the same cases as in Figure 7 of the shear load $\Sigma_h(t)$ applied by the piston.

Cf. the caption of that figure for an explanation of the different line-types. For the case corresponding to $U_h = 0$, we have $\Sigma_h \equiv 0$. The horizontal line $\Sigma_h = \Sigma_\infty$ corresponds to the asymptotic load in the purely plastic simulations.

identically zero, and we have from Eq. 37 that $\lim_{t\to\infty}\sigma_d^{yy} = \sigma_c(\phi_\infty) = \Sigma_v$. It follows that the asymptotic limit concentration, denoted ϕ_∞, is uniquely determined by the vertical load, and that it is necessarily homogeneous. Conservation of mass yields the asymptotic distance between the plates, H_∞. Further, we conclude that the network shear stress τ_d^{xy} will asymptotically everywhere approach the same constant value, namely $\tau_c(\phi_\infty)$. In a purely plastic case, it follows from Eq. 36 that this is also the value of the asymptotic shear load applied by the piston, whereas in the visco-plastic case the applied load must be larger to overcome the viscous resistance to deformation, i.e., $\Lambda\tau_{Nd}^{xy}$.

Since $\Lambda \ll 1$, the influence of the viscous stresses in the balance Eqs. 36 and 37 is however small. Including viscous stresses in any of the purely plastic simulations in Figures 7 and 8 would not change the corresponding curves significantly. When trying to explain the effects of the applied shear load on the rate of the consolidation process, we can therefore neglect the viscous terms in Eqs. 36 and 37. Now, consider some position in the flocculated network where the concentration is ϕ, which according to Eq. 42 corresponds to a yield-surface of a certain "size" (e.g., the one seen in Figure 2). If $\tau_d^{xy} = 0$, the capacity of the network to carry a vertical load is given by the intersection between the yield-surface and the σ_d^{yy} -axis. If a shear load is applied so that $\tau_d^{xy} \neq 0$, the ability of the network to support the vertical load is smaller. From Eq. 37 we can therefore conclude that if the suspension is subjected to a shear load in addition to the vertical load, a larger part of the latter must be balanced by the liquid pressure, i.e., the pore pressure increases. The result is an increased drainage rate, as seen in Figure 7. The effect should become more pronounced for higher shear loads, which is confirmed by the results in Figures 7 and 8. The evolution of the concentration profiles in the gap between the plates is not presented for the considered cases, as they are qualitatively similar to those obtained during uniaxial consolidation processes.

It is interesting that, in the absence of viscous stresses, different asymptotic velocity fields (given by different horizontal velocities U_h) correspond to the same asymptotic piston load $\lim_{t\to\infty}(\Sigma_v(t), \Sigma_h(t))$. By consequence, with the purely plastic model, the deformation-rates are dependent on the history of the load process. The same conclusion cannot be drawn about the viscous model, where the contribution from the rate-dependent stresses yields a different asymptotic load $\Sigma_h(t\to\infty)$ for each value of U_h.

Figure 9 contains horizontal velocity profiles at different instants for one visco-plastic and one purely plastic case. For numerical reasons it was not possible to continue the purely-plastic simulation beyond $t = 0.057$, and there is thus one less purely plastic profile than there are visco-plastic ones in the figure. In both simulations, the suspension close to the piston initially translates like a stiff cake, and it is only in the region next to the filter that the strain rates are finite. However, the region in which deformations of the suspension

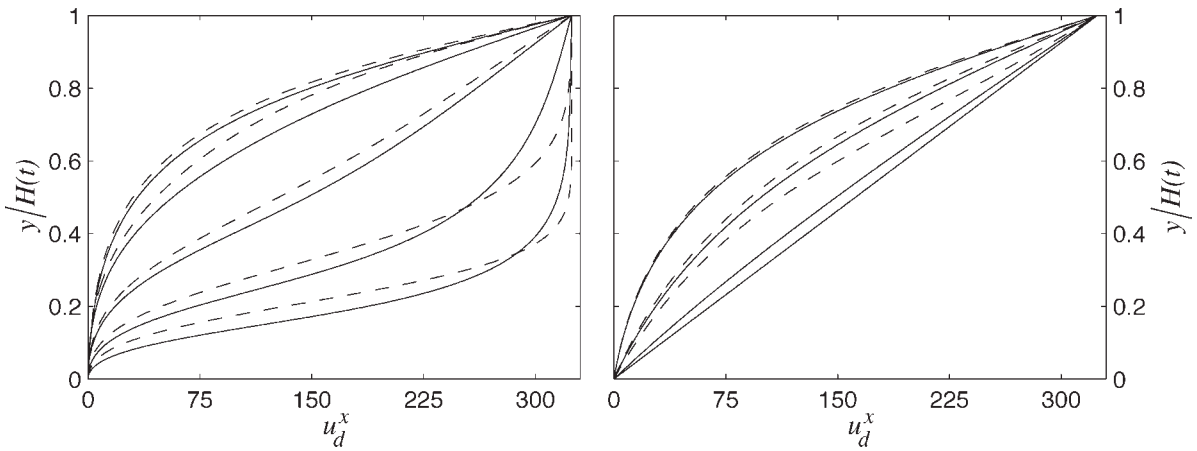

Figure 9. Comparison between visco-plastic (solid lines) and purely plastic (dashed lines) velocity profiles when Σ_v and U_h are kept at constant values (1 and 324, respectively).

Only $\tau_{Nd}^{xy} \neq 0$. Left subfigure: $t/10^{-3} = 0.5, 0.9, 1.8, 3.5, 7$. Time increases with distance from bottom right corner. Right subfigure: $t/10^{-3} = 14, 28, 57, 100$. Time increases with distance from top left corner. Only the visco-plastic profile is plotted for the largest time. $\Lambda = 5.6 \times 10^{-2}$.

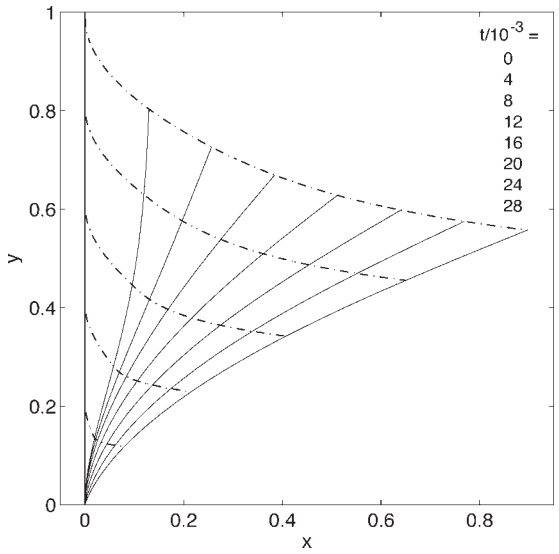

Figure 10. The deformation of a material line in the flocculated network.

At $t = 0$, the vertical load and the horizontal velocity of the piston are suddenly increased to $\Sigma_v = 1$ and $U_h = 32.4$, respectively, and then held constant. The material line is initially vertical, and is illustrated by the solid curves at the instants stated in the figure. The dash-dotted lines are particle trajectories.

structure occur grows progressively, till it fills the entire gap. At the instants of the last of the profiles, plots of the quantities $H(t)$ and $\Sigma_h(t)$ would reveal that the concentration and the piston loads are very near their asymptotic values. The systems are then hence very close to being at critical state everywhere. As seen in Figure 9, the asymptotic velocity profile in the purely plastic case does not appear to approach a linear shape, and as the horizontal strain-rate is absent from the force balance when $\Lambda = 0$ (cf. Eq. 36), there is no reason that it should. The situation is different in the presence of a non-zero viscous stress τ_{Nd}^{xy} Since the solid stress $\tau_d^{xy}(y, t\to\infty)$ equals the constant value $\tau_c(\phi_\infty)$, it follows from Eq. 36 that viscous stress τ_{Nd}^{xy} must be spatially constant, which in turn implies the same for the only nonzero strain-rate e_d^{xy} since it uniquely determines τ_{Nd}^{xy}. The visco-plastic model hence results in a linear velocity profile, as seen in Figure 9. A warning should be issued, however. The visco-plastic profile at $t = 0.057$, which corresponds to the last of the purely plastic profiles, is not perfectly linear. Hence, the visco-plastic simulation has at that point not yet reached the asymptotic state. It is likely that the same is true of the purely plastic calculation, and we therefore do not know the precise shape of $\lim_{t\to\infty} u_d^x(y, t)$ in this case. However, the difference between the purely plastic and the visco-plastic profiles at $t = 0.057$ is significantly larger than at earlier instants. This could indicate that the purely plastic solution is close to its asymptotic shape, since it evolves at a markedly lower pace than the visco-plastic counterpart.

The horizontal deformation of the network that occurs during sheared consolidation is of interest to some applications where it is desirable to smear out inhomogeneities in the particle concentration, e.g., paper manufacturing. Figure 10 therefore shows the deformation of an initially straight vertical material line in the flocculated network, for one of the purely plastic simulations. Some particle trajectories are also plotted.

Finally, it is appropriate to make a short comment on the scaling. Only the purely plastic case is considered, the viscous case is commented upon in the Appendix. From the work on uniaxial pressure filtration by Landman et al.[10] we know that some of the scales introduced in this study are only relevant after sufficiently long times. Those researchers find that, when no shearing is done and at small times, the true length and velocity scales of the problem are a fraction $\sqrt{t}$ and $1/\sqrt{t}$, respectively, of those presently used. The result should carry over to sheared consolidation, provided the employed loads $\Sigma_h(t)$, and consequently τ_d^{xy}, are small in comparison with the vertical stresses σ_d^{yy}. As this is the case at the initial stages of the process, it immediately explains the initially high downward velocity of the piston in Figure 7. Consider now the situation where the horizontal piston velocity is set to a constant value U_h. The integral in Eq. 64 evaluated at the piston is then constant. The diffusivity, defined by Eq. 58, is not affected by the differing initial scales, and we therefore conclude, based on our knowledge of the behavior of the length scale, that the function $g(\phi, \Sigma_h(t))$ should scale with $\sqrt{t}$ at small times. From Eqs. 56 and 62, it follows that τ_d^{xy}, and consequently $\Sigma_h(t)$, must do so as well, which explains the rapid increase of the loads in Figure 8. This is confirmed by the logarithmic plots of the small time behaviour of $\Sigma_h(t)$ in Figure 11.

Discussion

A characteristic of the inviscid critical state plasticity theory is that, when the solid structure attains critical state, deviatoric deformations occur at an undefined rate. In the present study this was exemplified by the observation that

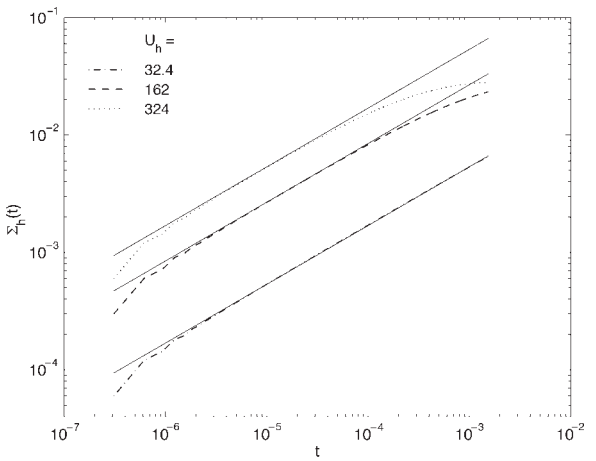

Figure 11. The small time behavior of the horizontal piston load $\Sigma_h(t)$ in the purely plastic simulations presented in Figure 8.

The corresponding solid lines are plots of $\Sigma_h(t) = 5.22U_h\sqrt{t}$. Values for U_h are stated in the figure. Note that the dimensionless time step $\Delta t = 3.1 \times 10^{-7}$, and that the smallest time scales are not resolved.

the asymptotic velocity field is dependent on the load history in the purely plastic simulations of piston driven filtration. In the original field of application of the theory, soil mechanics, relatively little attention has been paid to the evolution of the system once the critical state is attained, as this usually represent failure of the structure under consideration. During sheared consolidation, it is however difficult to disregard from the behavior of the suspension when the particle network reach critical state. By including viscous stresses, in addition to the plastic stresses, the deformation-rates become well-defined also at the critical state. In the present study, viscous stresses of Newtonian character are attributed to the particle phase. Although the scaling analysis reveals that these rate-dependent stresses are small in comparison to the solid stresses, it is nevertheless seen that they effectively resolve the issue of undefined deformation rates when some part of the flocculated network attains critical state. An additional benefit is that they improve the stability of the numerical algorithm. The simulations revealed that there was a limit to how close to critical state the system could get using the algorithm for the purely-plastic model. In a more complex situation than the one treated here, the need to prevent a break-down of the model because of the undefined behavior at critical state is even larger, since it is then difficult to conclude *a priori* if the system at some point will reach critical state or not.

Inertial effects were neglected in the analysis. This is common practice in studies of uniaxial compression,[12] and during piston driven consolidation it is normally motivated during the predominant part of the process. The exception is at the onset of the loading, when a finite force that is suddenly applied to the piston can yield very high drainage velocities if the resistance of the filter is low (indeed, a perfectly permeable filter yields an infinite velocity at $t = 0^+$). The inertial terms in the horizontal direction can be estimated by considering the quantity

$$\left(\frac{\rho_d U_0 H_0}{\mu_c}\right)\left(\frac{l}{H_0}\right)^2\left(\frac{\partial u_d^x}{\partial t} + u_d^y\frac{\partial u_d^x}{\partial y}\right), \tag{65}$$

where ρ_d is the density of the solid constituent (we here choose to focus on the particle phase, but this is of no importance if the solid and the liquid are of comparable densities and are displaced at similar rates). Naturally, the presence of the factor u_d^y in the third term might result in significant inertial effects at the onset of the consolidation process for the reasons explained above. During the remaining part of the compaction process, inertia can usually be neglected also in the horizontal direction.

Conclusion

Previously, the concept of a particle concentration dependent yield-stress has been used to model uniaxial consolidation of flocculated suspensions.[7,10] The present work generalizes the yield-stress concept to comprise flocculated phase shear strength. It is found that the evolution of the volume fraction of solids quantitatively exhibits the same behavior as during uniaxial consolidation. The treatment of the piston driven consolidation process reveals, however, that applying a shear load increases the rate of the dewatering because of the generation of higher pore pressures. Such an effect could in a real suspension be attributed to restructuring of the network, and increased loading of the inter-particle bonds due to the additional horizontal load component. The additional velocity component present during shearing is also interesting to applications, as it provides a way of influencing the morphology of the compressed solid phase, e.g., by smearing out inhomogeneities.

We have combined a plasticity model for the quasi-static yielding of soil, and incorporated it into a two-phase model for the flocculated suspension. Although here applied to one-dimensional compression, the approach should be possible to extend to more complex situations involving a dispersed solid phase possessing an inner strength. Some complications would appear, however. The reader's attention is directed to the assumption that the yield criterion is always fulfilled. As long as the load transmitted to the network is not relaxed at any material point, it is valid. In spatially one-dimensional problems, it is fairly straight-forward to ensure that the requirement is fulfilled by choosing appropriate external loads and initial conditions. However, in a general situation, a constitutive description is needed for the behavior of the suspension at stress states that are not located on the yield surface. The modeling choices made, in particular our choice of yield surface and the associated flow rule, were motivated by simplicity. Naturally, they have to be adapted to the suspension under consideration. Unfortunately, we are not aware of any experimental work that provides enough data to trace out the yield surface of a flocculated suspension in e.g., $\sigma_d^{yy} - \tau_d^{xy}$ space, let alone to determine the flow rule.

It is our hope that it will be possible to continue to draw upon the knowledge and models gathered in the field of soil mechanics to deal with other issues relevant to strongly flocculated suspensions, e.g. the effects of anisotropy.

Literature Cited

1. Kynch GJ. A theory of sedimentation. *Trans Faraday Soc*. 1952; 48:166–176.
2. Michaels AS, Bolger JC. Settling rates and sediment volumes of flocculated kaolin suspensions. *Ind Eng Chem Fundam*. 1962; 1(1):24–33.
3. Shirato M, Kato H, Kobayashi K, Sakazaki H. Analysis of settling of thick slurries due to consolidation. *J Chem Eng Jpn*. 1970;3:98–104.
4. Adorján LA. A theory of sediment compression. In: *11th International Mineral Processing Congress*. Cagliari, 1975:297–318.
5. Auzerais FM, Jackson R, Russel WB. The resolution of shocks and the effects of compressible sediments in transient settling. *J Fluid Mech*. 1988;195:437–462.
6. Davis KE, Russel WB. An asymptotic description of transient settling and ultrafiltration of colloidal dispersions. *Phys Fluids*. 1988;1(1):82–100.
7. Buscall R, White LR. The consolidation of concentrated suspensions, Part 1: the theory of sedimentation. *J Chem Soc Faraday Trans 1*. 1987;83:873–891.
8. Landman KA, White LR, Buscall R. The continuous-flow gravity thickener: steady state behaviour. *AIChE J*. 1988;34(2):239–252.
9. Howells I, Landman KA, Panjkov A, Sirakoff C, White LR. Time-dependent batch settling of flocculated suspensions. *Appl Math Model*. 1990;14:77–86.
10. Landman KA, Sirakoff C, White LR. Dewatering of flocculated suspensions by pressure filtration. *Phys Fluids A*. 1991;3(6):1495–1509.

11. Landman KA, Russel WB. Filtration at large pressures for strongly flocculated suspensions. *Phys Fluids A*. 1993;5(3):550–560.
12. Landman KA, White LR, Eberl M. Pressure filtration of flocculated suspensions. *AIChE J*. 1995;41(7):1687–1700.
13. Stickland AD, De Kretser RG, Scales PJ. Nontraditional constant pressure filtration behavior. *AIChE J*. 2005;51(9):2481–2488.
14. Stickland AD, White LR, Scales PJ. Modeling of solid-bowl batch centrifugation of flocculated suspensions. *AIChE J*. 2006;52(4): 1351–1362.
15. Barr JD, White LR. Centrifugal drum filtration. I. A compression rheology model of cake formation. *AIChE J*. 2006;52(2): 545–556.
16. Barr JD, White LR. Centrifugal drum filtration. II. A compression rheology model of cake draining. *AIChE J*. 2006;52(2): 557–564.
17. Buscall R, Mills PDA, Yates GE. Viscoelastic properties of strongly flocculated polystyrene latex dispersions. *Colloids Surf*. 1986;18: 341–358.
18. Buscall R, McGowan IJ, Mills PDA, Stewart RF, Sutton D, White LR, Yates GE. The rheology of strongly-flocculated suspensions. *J Non-Newtonian Fluid Mech*. 1987;24:183–203.
19. Channell GM, Zukoski CF. Shear and compressive rheology of aggregated alumina suspensions. *AIChE J*. 1997;43(7):1700–1708.
20. Gustavsson K. Mathematical and Numerical Modeling of 1-D and 2-D Consolidation. PhD Thesis. Stockholm, Sweden: Royal Institute of Technology (KTH), 2003.
21. Savage SB. Granular flows down rough inclines—review and extension. In: Jenkins JT, Satake M, editors. *Mechanics of Granular Materials: New Models and Constitutive Relations*. Amsterdam: Elsevier, 1983;261–282.
22. Johnson PC, Jackson R. Frictional-collisional constitutive relations for granular materials with application to plane shearing. *J Fluid Mech*. 1987;176:67–93.
23. Johnson PC, Nott P, Jackson R. Frictional-collisional equations of motion for particulate flows and their application to chutes. *J Fluid Mech*. 1990;210:501–533.
24. Wood DM. *Soil Behaviour and Critical State Soil Mechanics*. Cambridge: Cambridge University Press, 1990.
25. Zhao J, Wang C-H, Lee D-J, Tien C. Plastic deformation in cake consolidation. *J Colloid Interface Sci*. 2003;261:133–145.
26. Owen DRJ, de Souza Neto EA, Zhao SY, Perić D, Loughran JG. Finite element simulation of the rolling and extrusion of multiphase materials application to the rolling of prepared sugar cane. *Comput Methods Appl Mech Eng*. 1998;151:479–495.
27. Ungarish M. *Hydrodynamics of Suspensions*. Berlin: Springer-Verlag, 1993.
28. Ingmanson WL, Andrews BD, Johnson RC. Internal pressure distributions in compressible mats under fluid stress. *Tappi J*. 1959; 42(10): 840–849.
29. Roscoe KH, Burland JB. On the generalised stress-strain behaviour of 'wet' clay. In: Heyman J, Leckie FA, editors. *Engineering Plasticity*. Cambridge: Cambridge University Press,1968:535–609.
30. Amberg G, Tönhardt R, Winkler C. Finite element simulations using symbolic computing. *Math Comput Simulat*. 1999;49:257–274.
31. Zahrai S, Martinez MD, Dahlkild A. Estimating the thickness of the web during twin-wire forming. *J Pulp Paper Sci*. 1998;24(2):67–72.
32. Paradis MA, Genco JM, Bousfield DW, Hassler JC, Wildfong V. Measurement of drainage under conditions of known shear rate. *J Pulp Paper Sci*. 2003;29(12):395–400.

Appendix

Incorporating viscous stresses

When viscous stresses are present, the treatment of the piston-driven case need to be modified as described below.

By limiting ourselves to situations in which $\tau_d^{xy} \geq 0$, we can rewrite Eq. 42 as a relation for τ_d^{xy},

$$\tau_d^{xy} = h(\phi, \sigma_d^{yy}). \tag{A1}$$

When Eq. 56 is rewritten in the following form, it is valid also at the critical state $\sigma_d^{yy} = P_0(\phi)/2$,

$$M^2\left(\sigma_d^{yy} - \frac{1}{2}P_0(\phi)\right)e_d^{xy} + \left(1 + \frac{2}{3}M^2\right)\tau_d^{xy}e_d^{yy} = 0. \tag{A2}$$

Adopting a Newtonian description for the rate-dependent particle stresses (a choice made arbitrarily for modeling simplicity) one has the nonzero viscous stress components

$$\tau_{Nd}^{xy} = 2e_d^{xy}, \tag{A3}$$

$$\tau_{Nd}^{yy} = \frac{4}{3}e_d^{yy}. \tag{A4}$$

A viscous counterpart to equation Eq. 57 for the concentration is obtained by combining Eqs. 39, 55, and A4 into

$$\frac{\partial\phi}{\partial t} + U_v(t)\frac{\partial\phi}{\partial y} - \frac{\partial}{\partial y}\left(\phi(1-\phi)K(\phi)\frac{\partial}{\partial y}\left(\sigma_d^{yy} - \frac{4\Lambda}{3}e_d^{yy}\right)\right) = 0. \tag{A5}$$

Again using Eqs. 39 and A4, this time with the result Eq. 63, yields an equation for the normal deformation-rate,

$$e_d^{yy} + \frac{\partial}{\partial y}\left((1-\phi)K(\phi)\frac{\partial}{\partial y}\left(\sigma_d^{yy} - \frac{4\Lambda}{3}e_d^{yy}\right)\right) = 0. \tag{A6}$$

In addition, Eqs. 36, A1, A2, and A3 can be used to derive the following algebraic equation, connecting the dependent variables in Eqs. A5 and A6,

$$M^2\left(\sigma_d^{yy} - \frac{1}{2}P_0(\phi)\right)\frac{\sum_h(t) - h(\phi, \sigma_d^{yy})}{2\Lambda} + \left(1 + \frac{2}{3}M^2\right)h(\phi, \sigma_d^{yy})e_d^{yy} = 0. \tag{A7}$$

Consider now the boundary conditions needed to solve Eqs. A5 and A6, assuming that the piston is load-controlled. From Eqs. 1, 37, and A4, we find that the following condition must be fulfilled at the filter,

$$\left[\sigma_d^{yy} - \frac{4\Lambda}{3}e_d^{yy}\right]_{y=0} = \Sigma_v(t). \tag{A8}$$

At the other end of the domain, the vertical velocity of both phases are equal to the velocity of the piston, i.e., $j_r^y = 0$, and Eq. 39 tells us that

$$\left[\frac{\partial}{\partial y}\left(\sigma_d^{yy} - \frac{4\Lambda}{3}e_d^{yy}\right)\right]_{y=H(t)} = 0. \tag{A9}$$

When the piston is load-controlled, its velocity components need to be solved for, notably $U_v(t)$ which appears explicitly in Eq. A5. Using the condition Eq. 2, which corresponds to $\boldsymbol{j}_d = 0$ at the filter, and the result Eq. 35 in Eq. 9, we get a relation for the vertical piston velocity,

$$U_v(t) = -\left[\frac{j_r^y}{\phi}\right]_{y=0} = \left[(1-\phi)K(\phi)\frac{\partial}{\partial y}\left(\sigma_d^{yy} - \frac{4\Lambda}{3}e_d^{yy}\right)\right]_{y=0}. \tag{A10}$$

The horizontal component of the solid phase velocity, u_d^x, can be obtained by first calculating the velocity gradient $\partial u_d^x/\partial y$ from Eqs. 20, 36, A1, and A3, and then integrating in the direction away from the filter, revealing

$$u_d^x(y,t) = \int_0^y \frac{\sum_h(t) - h(\phi, \sigma_d^{yy})}{\Lambda} dy', \qquad \text{(A11)}$$

where the condition $u_d^x(0,t) = 0$ has been used. As $j_r^x = 0$, Eq. A11 also provides the horizontal liquid phase velocity, as well as the corresponding mixture flux density component j^x. Further, the piston velocity in the x-direction is $U_h(t) = u_d^x(H(t),t)$.

When the piston velocity is directly controlled, Eq. A9 is still used as a boundary condition. However, the Eq. A10 replaces Eq. A8 as the condition applied at the filter. The shear stress appearing in the equations is obtained by solving Eq. A11, evaluated at $y = H(t)$, for $\Sigma_h(t)$ as a function of $U_h(t)$. The necessary vertical load $\Sigma_v(t)$ is determined *a posteriori* from Eq. A8.

Frequently, we have also chosen to specify the combination $\Sigma_v(t)$ and $U_h(t)$, in which case Eqs. A8–A10 are used as in the load-controlled case, but the necessary shear stress $\Sigma_h(t)$ is determined as in displacement-controlled simulations.

To prevent a break-down of the model when some point of the flocculated phase reaches critical state, it is in our particular plane-strain problem only necessary to include the stress component τ_{Nd}^{xy}. The governing equations for this situation can be obtained from those presented above, by simply inserting $\tau_{Nd}^{yy} = 0$. Practically, this amounts to removing the group $4e_d^{yy}/3$ at all occurrences.

The scales at small times differ from those obtained in the purely plastic case. Assume first that only $\tau_{Nd}^{xy} \neq 0$, as in the presented simulations. It then follows from Eq. A5 that the length scale of the deforming region next to the filter and $U_v(t)$ scale as $\sqrt{t}$ and $1/\sqrt{t}$, respectively. Consequently, in this region, e_d^{yy} behaves as $1/t$, and, if we assume that the horizontal velocity is ramped linearly, e_d^{xy} as $\sqrt{t}$. From Eq. A2, we conclude that τ_d^{xy} scales as $t\sqrt{t}$, which is a factor t smaller than in the inviscid case. Finally, Eq. A7 requires that $\Sigma_h(t)$ increases as $\sqrt{t}$, i.e., the same as in the purely plastic case. Note that the viscous stress τ_{Nd}^{xy} is a factor $1/t$ larger than the rate-independent stress τ_d^{xy}. If also $\tau_{Nd}^{yy} \neq 0$, a similar analysis would reveal that $U_v(t)$, e_d^{yy}, and τ_d^{xy} scale as $\sqrt{t}$, 1 and $\sqrt{t}$, respectively. The other quantities retain their behaviors. Note that in the essentially non-deforming larger region next to the piston, the horizontal load at small t is balanced by $\tau_d^{xy} = \Sigma_h(t)$, whereas τ_{Nd}^{xy} is zero.

Manuscript received Mar. 16, 2007, and revision received Nov. 30, 2007.